Polarization Dynamics in Vertical-Cavity Surface-Emitting Lasers with Optical Feedback: Experiment and Model

M. Giudici[1], T. Ackemann[1,2], S. Barland[1], J. R. Tredicce[1], and S. Balle

Dept. de Física Interdisciplinar,

Instituto Mediterráneo de Estudios Avanzados, IMEDEA (CSIC-UIB),

E-07071 Palma de Mallorca, Spain

[1] *Also at Institut Non Linéarie de Nice, CNRS UMR 6618, 06560 Valbonne, France*

[2] *Permanent address: Institut für Angewandte Physik, Univ. of Münster, Münster, Germany*

(vcsel02.tex, April 1, 1998)

Abstract

We study the polarization resolved dynamics of a VCSEL with mode-matched and unpolarized optical feedback. The total power can display Low-Frequency Fluctuations which are associated with drops in power of the dominant linearly polarized mode and bursts in the power of the depressed one. However, for most parameter values the VCSEL output does not display Low-Frequency Fluctuations, although antiphase dynamics among the two linear polarization components has been found. A theoretical model that includes all reflections in the external cavity with a minimum computational cost is developed.

I. INTRODUCTION

Optical feedback from an external reflecting surface has a strong impact on the output characteristics of edge-emitter semiconductor lasers, hence it has been the subject of extensive research both theoretically and experimentally [1]. Optical feedback is characterized by three main parameters: *i)* the amount of optical power fed back into the laser cavity, which is mainly controlled by the effective reflectivities of the laser facet and the external surface, *ii)* the feedback phase, which can be controlled by submicrometer adjustments of the position of the reflecting surface, *iii)* the round-trip time of the optical field in the external cavity. Depending on these parameters and the current injected into the laser diode, different regimes can be found [2]. Low or high enough feedback levels can stabilize the emitted optical field, thus yielding a linewidth reduction [3]. However, in a large range of parameter values the system may show strong fluctuations of the intensity and the linewidth becomes broad up to a point that several authors name such dynamical behavior as "coherence collapse" [4].

Vertical-Cavity Surface-Emitting Lasers (VCSELs) have been developed during the last years, and they are becoming increasingly popular because they offer inherent advantages over edge-emitting lasers — such as single-longitudinal mode operation, circular output beam, low threshold current and large-scale integrability in two-dimensional arrays. Thus, VCSELs are particularly interesting for both basic research and technological applications [6].

Due to the short cavity length of VCSELs ($\sim 1\mu m$) the longitudinal mode spacing is of the order of 40 THz ($\sim$ 100 nm for VCSELs emitting around 0.8μm) thus allowing the VCSEL to oscillate in a single longitudinal mode although the width of the gain curve is typically $\sim$ 50 nm [7]. Nevertheless, the transverse dimensions of VCSELs in general allow for several transverse modes, hence VCSELs operate in single-mode only over a limited range of injection currents. Due to their short cavity length and to the even much shorter active medium, very high reflectivity mirrors ($R \sim 99\%$) are required in order to reduce the threshold current to practical values. Moreover, the emission of VCSELs is usually polarized along one of the crystal axes, but they often exhibit a sudden 90^o change in the orientation of the emitted optical field, while keeping operation in the fundamental transverse mode [8], a phenomenon called polarization switching.

It has been argued that VCSELs should be relatively immune to optical feedback due to high reflectivity of the mirrors forming the cavity [9,10]. However, it has been shown that VCSELs may exhibit in some cases a sensitivity to optical feedback comparable to that of edge-emitter lasers [11,12]. There is an obvious interest on the effects of optical feedback on VCSELs due to their practical implications. Several studies have focused either on the dynamics of the total power emitted by the device [9–12] or on the dynamics of the transverse modes [13,14]. Recent studies have shown that coupling the VCSEL to an external cavity which contains a $\lambda/4$-waveplate can induce polarization self-modulation of the VCSEL emission [15–18].

In this paper we show that a VCSEL with non-polarizing, mode-matched optical feedback can display instabilities in the total output power which are linked to fluctuations in the polarization components of the VCSEL emission. We show that for perfect phase matching and alignment of the external cavity, the total output power is quite stable over a wide range of parameter values, although anti-phase oscillations of the two linear polarization components may occur, with a oscillation period corresponding to the external cavity round-trip time. As the current injection is increased, instabilities of the total output power which look like the well known Low-Frequency Fluctuations in edge-emitting lasers develop. Fluctuations appear simultaneously in the two polarization modes, in such a way that the dominant polarization mode displays power drops which are simultaneous with bursts in the power of the depressed polarization mode. A theoretical model is presented which satisfactorily explains the experimental results. The model is based on the Spin-Flip Model (SFM) [19]. In order to describe the effects of the external mirror we develop an approximation valid for arbitrary reflectivities of the external mirror which includes all round-trips in the external cavity [14]. The widely used Lang and Kobayashi approximation [21], which accounts only for one round-trip in the external cavity, is recovered in the limit of very low optical feedback.

The paper is organized as follows. In Sect. II we present the experimental results. In Sect. III we develop the model, and in Sect. IV we analyze the numerical results and we compare them with experimental ones. Sect. V summarizes our work.

II. EXPERIMENTAL RESULTS

In our study, we use a proton-implanted GaAs VCSEL with lasing wavelength λ_0 around 850 nm manufactured by VIXEL Corporation. The active area is defined by proton implantation, its diameter is around 8μm [22]. The VCSEL is battery powered and mounted on a thermo-electric device to stabilize the temperature. The VCSEL output is focused by an AR-coated aspheric lens onto a distant reflector that provides mode-matched optical feedback. Two different configurations of the external cavity have been used. The first one allows for high feedback (threshold reduction of 28%, Fig. 1). The second one —where mirror M in Fig. 1 was removed and BS1 was substituted by a wedged glass substrate— provides intermediate feedback (threshold reduction of 15%). These configurations have been chosen in order to avoid interferometric effects from any optical elements. In fact, the symmetric beam shape of the VCSEL together with its high spectral purity easily produce interference effects in optical elements with parallel faces (beam splitters, dielectric mirrors, windows, neutral density filters, etc.), which act as an etalon if anti-reflection coatings are not perfect. This effect has to be avoided in order to maintain the feedback not selective in frequency. Moreover, the incidence of the beam onto the surfaces of the optical elements should be normal in order to preserve the polarization in the external feedback cavity.

The output is polarization-resolved by means of a Glan-Taylor prism. A half waveplate placed into the optical path just before the Glan-Taylor prism allows to check the orientation of the analyzer with respect to the polarization emitted by the laser. Thus, a rotation of the polarization axis of the output field can be measured and compensated for by rotating the half-waveplate. The two beams emerging from the polarizer are focused onto Si avalanche photodetectors (APD1 and APD2, bandwidth $\approx 2.5\ GHz$). Their signals are monitored with a digital oscilloscope (LC 7200A, analog bandwidth 500 MHz). An RF-spectrum analyzer monitors the power spectrum of the signals in a range covering the full bandwidth of the detectors. The optical spectrum is obtained with a scanning Fabry-Perot whose free spectral range is 293 GHz, and its finesse is of the order of 200.

The main characteristics of the solitary VCSEL are shown in Fig. 2. The threshold current of the solitary VCSEL is $I_{th}^{sol} = 2.65\ mA$, and it emits linearly polarized light in the fundamental transverse mode up to 3.7 mA. For currents between 3.7 mA and 4.4 mA, we have bistability between the two linearly polarized modes with noise-induced switching from one to the other, whose frequency splitting is of the order of 2.8 GHz. Above 4.4 mA, the first order transverse mode appears.

In the feedback experiment we will stay always well below this point. The aim of this work is to characterize the dynamical behavior of the VCSEL with feedback in the parameter region where the intensity output of each polarization component is not stable.

In Fig. 3 we show the polarization-resolved L-I curve of the VCSEL with high feedback. The threshold is now $I_{th} = 1.9\ mA$, and the emission is stable and linearly polarized for currents above $I_1 = 2.22\ mA$. At $I \sim 2.65\ mA$, a polarization switching occurs, but the laser emission is still stable and linearly polarized until the higher order transverse mode comes into play.

For currents between I_{th} and I_1 the VCSEL output is unstable both in total power and polarization orientation. Close to I_{th} (see Fig. 4, $I = 2.07\ mA$), the output field is almost linearly polarized but there are important fluctuations at low frequency in the two components. The power spectrum of each component shows multiple beat notes of external cavity modes, and noise excess at low frequencies. For higher currents (Fig. 5, $I = 2.17.\ mA$) the amplitude of the low frequency fluctuations increases, and the two polarization components are in anti-phase.

At this point the fluctuations manifest themselves in sudden drops in the power of the dominant polarization component (and the total power) which is followed by a rather slow stepwise recovery. This shape resembles very much the shape of the power drops in the low frequency fluctuation regime in edge emitters with feedback. Each drop of power of the dominant polarization component is accompanied by a burst in power of the one which is usually depressed.

Further increasing the current, the low frequency fluctuations appear grouped in bursts

(Fig. 6, $I = 2.21\ mA$) separated by intervals of constant output. The length of the bursts reduces and the time between bursts increases as the current is increased.

Finally, for currents above I_1 the low frequency fluctuations disappear and the output is linearly polarized. However, the RF spectrum of each polarized component displays several narrow peaks with side-bands at multiples of the external cavity frequency spacing (see top and bottom traces in Fig. 7). The two linearly polarized components can be adjusted to interfere with variable amplitude by rotating the half-waveplate. We observe that the RF spectrum is modified by this operation, and there is a position of the half-waveplate where the central component of the external cavity modes is suppressed while the side-bands remain (Fig. 7). This result indicates that each polarization is oscillating with a period corresponding to the external round trip time but in anti-phase, because the beating disappears if we compensate their difference in amplitude. The side-bands indicate that a second lower frequency exists and the two polarization components oscillate in-phase at this frequency. For currents above 2.65 mA, the system then emits linearly stable on the other component and single external cavity mode operation is improved if the current is further increased.

It is worth remarking that the orientation of the polarization axes of the VCSEL with feedback is affected by minute anisotropies in the external cavity. As a consequence, the emission of the VCSEL with feedback has in general principal axes rotated with respect to those of the solitary device. This uncontrolled rotation of the axes can be compensated for by the $\lambda/2$ wave-plate in the output beam thus realigning the emission axes with those of the polarizer. Interestingly, the orientation of the linearly polarized emission from the VCSEL with feedback can be controlled by inserting a highly anisotropic element in the external cavity (as a $\lambda/4$ or $\lambda/2$ waveplate), whose axes become dominant.

In Figs. 8 and 9 we show the intermediate feedback case. In this case the output of the system is always very noisy with broad peaks in the power spectrum both at low frequency and at the external cavity resonances. Although antiphase dynamics is not as clear as for the strong feedback case, anyway it is clear that the fluctuations in both polarizations are synchronous.

III. MODEL

In order to describe the effects of optical feedback on the output characteristics of the VCSEL, we have on one hand to describe the interaction of the optical field with the material in the active region, and on the other, we have to include in the description the effects of the external mirror while keeping the vectorial caracter of the optical field.

Our starting point for the description of the VCSEL is the Spin-Flip Model (SFM) developed in [19]. The main characteristic of the SFM is the consideration of the carrier's spin dynamics as a source of polarization instabilities: the carrier density is decomposed into two subsets (associated with spin-up and spin-down carriers, respectively) which are coupled among them by spin-flip relaxation processes, and which interact with the circularly right- and left-polarized components of the optical field.

The SFM is complete by adding a rate equation for the evolution of each component of the optical field; the SFM has been extensively studied, and it allows to satisfactorily explain the polarization switchings that occur in VCSELs [20]. However, the original SFM model does not include optical feedback, and therefore the evolution equations for the optical field have to be modified in order to take it into account. Polarized feedback effects in the SFM have been considered previously by adding to the rate equations for one of the field components a delayed term which represents the effect of the external mirror [17,15]. For unpolarized feedback one could follow the same approach for both components of the field; however, in this limit only one roundtrip in the external cavity is taken into account for the dynamics, and it has been pointed out [14,23] that due to the high reflectivity of the Bragg mirrors defining the VCSEL cavity, several roundtrips should be considered. Nevertheless, as shown in the Appendix, an approximation taking into account all roundtrips in the external cavity can be developed for any reflectivity of the external mirror based on the fact that the Bragg mirror reflectivity is almost one.

In this approximation, the dynamical evolution of the system is given by

$$R_\pm(t) = \frac{c}{2n_g L}\hat{r}_3 \frac{1-r_2^2}{r_2} A_\pm(t-\tau) - r_2 \hat{r}_3 R_\pm(t-\tau) \ , \tag{1}$$

$$d_t N_\pm = \frac{I}{2eV} - \gamma_e N_\pm - 2g\frac{N_\pm - N_t}{1+s|A_\pm|^2}|A_\pm|^2 - \gamma_J (N_\pm - N_\mp) \ , \tag{2}$$

where

$$R_\pm(t) = d_t A_\pm(t) + \kappa A_\pm(t) + (\gamma_a + i\gamma_p)A_\mp(t) - \Gamma g(1-i\alpha)\frac{N_\pm - N_t}{1+s|A_\pm|^2}A_\pm \ . \tag{3}$$

In these equations, $A_\pm$ is the slowly varying amplitude of the left and right circularly-polarized components of the optical field, and $N_\pm$ is the carrier density with spin-down and up, respectively. In addition, $\kappa = 1/(2\tau_p)$ (τ_p being the photon lifetime in the solitary VCSEL cavity), g is the differential material gain multiplied by the group velocity of the transverse mode, c/n_g, N_t is the transparency carrier density, s is the gain saturation parameter, α is the linewidth enhancement factor, Γ is the field confinement factor to the active region, and γ_a and γ_p are the dichroism and birefringence, respectively. $\hat{r}_3 = r_3 e^{i\Omega\tau}$ is the amplitude reflection coefficient into the VCSEL cavity including the optical phase change after one external cavity roundtrip. $I/(2eV)$ is the density of carriers with given spin orientation injected into the active region per unit time, γ_e is the nonradiative carrier relaxation rate, and γ_J is the spin-flip rate.

It is worth noting that (1) and (2) reduce to the SFM model when there is no external cavity [$R_\pm(t) = 0$], and that the Lang and Kobayashi approximation is recovered in the limit of weak feedback, when only the first round-trip in the external cavity needs to be taken into account,

$$\begin{aligned} R_\pm(t) &= \frac{c}{2n_g L}\hat{r}_3 \frac{1-r_2^2}{r_2} A_\pm(t-\tau) - r_2 \hat{r}_3 R_\pm(t-\tau) \\ &= \frac{c}{2n_g L}\hat{r}_3 \frac{1-r_2^2}{r_2} A_\pm(t-\tau) - r_2 \hat{r}_3 \frac{c}{2n_g L}\hat{r}_3 \frac{1-r_2^2}{r_2} A_\pm(t-2\tau) + ... \\ &\approx \frac{c}{2n_g L}\hat{r}_3 \frac{1-r_2^2}{r_2} A_\pm(t-\tau) \ . \end{aligned} \tag{4}$$

Moreover, from the numerical point of view they allow us to approximately describe the effect of all reflections in the external mirror with a single additional memory vector, $R_\pm(t-\tau)$, thus memory consumption and computational cost are essentially the same as in the Lang and Kobayashi approximation.

Equations (1) and (2), together with (3), can be recast into the form used in [20] by scaling the variables according to

$$E_{\pm} = \sqrt{\frac{\kappa}{\Gamma\gamma_e}} A_{\pm} \ , \tag{5}$$

$$N = \Gamma\frac{g}{\kappa}\left(\frac{N_+ + N_-}{2} - N_t\right) \ , \tag{6}$$

$$n = \Gamma\frac{g}{\kappa}\frac{N_+ - N_-}{2} \ . \tag{7}$$

We also include spontaneous emission noise and injection current fluctuations into the evolution equations, which then read

$$R_{\pm}(t) = \kappa f E_{\pm}(t-\tau) - r_2\hat{r}_3 R_{\pm}(t-\tau) + \sqrt{\beta(N \pm n)}\chi_{\pm}(t) \ , \tag{8}$$

$$d_t N = \gamma_e\left(\mu - N - \frac{N+n}{1+s'|E_+|^2}|E_+|^2 - \frac{N-n}{1+s'|E_-|^2}|E_-|^2\right) + \sqrt{\varepsilon}\chi_N(t) \ , \tag{9}$$

$$d_t n = -\gamma_s n - \gamma_e\left(\frac{N+n}{1+s'|E_+|^2}|E_+|^2 - \frac{N-n}{1+s'|E_-|^2}|E_-|^2\right) + \sqrt{\varepsilon}\chi_n(t) \ , \tag{10}$$

where

$$R_{\pm}(t) = d_t E_{\pm}(t) + \kappa E_{\pm}(t) + (\gamma_a + i\gamma_p)E_{\mp}(t) - \kappa(1-i\alpha)(N \pm n)\frac{E_{\pm}}{1+s'|E_{\pm}|^2} \ , \tag{11}$$

with the other parameters being given as $f = (c/\kappa 2n_g L)\hat{r}_3(1-r_2^2)/r_2$, $s' = \Gamma\gamma_e s/\kappa$ and $\mu = (\kappa/\Gamma g)\left[(I/2eV\gamma_e) - N_t\right]$. Finally, the Langevin terms $\chi_i(t)$ are taken as uncorrelated, gaussian white noises.

IV. NUMERICAL RESULTS

We have numerically integrated eqs. (8)-(11) for a variety of injection currents and different external cavity setups. The output of the VCSEL may exhibit a variety of behaviours depending on the injection current and the parameter values. We analyze here the evolution with current injection for quite a typical parameter set for the VCSEL [20] ($\kappa = 300\ ns^{-1}$,

$\alpha = 3$, $\gamma_e = 1\ ns^{-1}$, $L = 0.24\mu m$, $n_g = 3.5$, $r_2 = 0.998$, $r_1 = 1$, $\gamma_s = 50$, $s' = 0.1$, $\gamma_p = 35\ ns^{-1}$, $\gamma_a = 0.1\ ns^{-1}$). For the noise strengths we take $\beta = \epsilon = 310^{-4}\ ns^{-1}$.

For an effective reflectivity of the external mirror $r_3 = 0.075$, a 12% maximum threshold reduction is achieved. Emission in a single polarization orientation, in either single or multiple external-cavity modes is found for currents close enough to threshold (see figure 10). As the current is increased, periodic switching among the two polarization orientations is found, the two polarizations being in an antiphase state which oscillates with a period corresponding to the external cavity roundtrip time (see figure 11).

Further increase of the injection current leads to a clearly unstable output of the VCSEL associated with irregular bursts of the depressed polarization mode (see figure 12). In this unstable regime, low-pass filtering of the VCSEL output displays power drops on a slow time scale corresponding to the time interval between bursts, which is of the order of $50 - 100ns$. The recovery time of these power drops is of the order of tens of ns, and both these time scales and the shape of the power drop and recovery time are very similar to the so called Low-Frequency-Fluctuations (LFF) observed in edge emitting lasers with optical feedback. Noteworthy, the polarization resolved filtered traces show that the drops in the total power coincide with drops in the power of the dominant polarization component and with an increase in the power of the depressed one; moreover, the depressed mode remains excited during times noticeably longer than the duration of the drop in the total power, thus leading to two-mode operation during most of the time. When one of the polarization modes is at the noise level, the VCSEL output is either stable or displays dynamics corresponding to multiple external-cavity mode operation. However, it does not exhibit power drops, which occur only when both polarization modes are active, although there are regimes where both are active and the VCSEL output is quiescent.

Since the two linear polarization components have a frequency splitting given by the residual birefringence, the time resolved spectrum in the LFF regime shows that total power drops correspond to a power drop in the dominant linear polarization component followed by a power increase in the depressed one, thus leading to a transfer of power from the former to the latter which survives quite longer than the total power drop. This effect has already been observed in edge emitting lasers with optical feedback in the LFF regime [24], although in this case many more than two modes are involved in the dynamics.

In addition, it is clear from figure 12 that the total power oscillates around a DC level and that it approaches the zero level when a power drop occurs. Therefore, the statistics of the total power on a fast time scale is peaked around the mean value of the power, and decreases for both high and low power levels (see figure 13). It is worth noting that the decrease on both sides of the maximum is controlled by the nonlinear gain saturation s', which forbids high power pulses and the subsequent depletion of carrier density which leads to a deep minimum in the total power; however, even for $s' = 0$ we find a power distribution peaked around its mean value, although the distribution in this case is broader. Similar results were found for edge-emitting lasers with optical feedback. [25,26]

For even higher currents (see figure 14) the drops become much more frequent, and the optical spectrum displays two peaks corresponding to each of the linear polarization components. Moreover, low power values become more frequent, and as a consequence the statistical distribution of the power flattens (see figure 15).

The dynamics obtained from the numerical simulations and its evolution as the current injection is raised is qualitatively similar to the experimental observations. The ambiguities in parameter values do not allow for quantitative comparisons, and make an exhaustive parameter space covering useless. However, we have checked that forcing the system to operate with the same density of spin-up and spin-down carriers (i. e., in the limit $\gamma_s \to \infty$) the results are qualitatively the same as when spin dynamics is included in the model. We have also considered the case of a VCSEL with very large dichroism, in such a way that in the absence of feedback only one of the polarization modes is stable in a very broad range of injection current, i. e., a quasi single-mode situation: the VCSEL is now much more stable, but in the unstable regions the phenomenology is the same as discussed previously although LFF appear at higher currents than before. Finally, we have performed deterministic simulations of the theoretical model; in this case we find that LFF occur at much higher currents as compared with the stochastic case. Moreover, the LFFs obtained in this case are much more irregular, and reminiscent of the so-called "coherence collapse", so it seems that noise leads to an anticipation of the onset of LFF through escape from an otherwise stable state.

The main point of disagreement between the theoretical model and the experimental observations concerns the point where LFF are obtained with respect to the solitary laser threshold. In the experimental results, LFF appear in a restricted current range below the solitary laser threshold. Instead, the numerical simulations do not display LFF until $\mu > 1$, i. e. above the threshold of the solitary VCSEL, although antiphase oscillations at the external cavity round-trip time may occur for $\mu < 1$. We think that the reason for such a discrepancy is likely to be that in the theoretical model the frequency dependence of the gain and refractive index (α-factor) have not been considered. The emission wavelength of the VCSEL with feedback is noticeably redshifted with respect to that of the solitary VCSEL, which may involve substantial changes in the VCSEL parameter values not taken into account in the theoretical model. The inclusion of such effects requires a dynamical model that includes the spectral dependences of both the gain and the linewidth enhancement factor, and is currently under investigation.

V. CONCLUSIONS

We have analyzed the polarization resolved dynamics of a VCSEL with mode-matched and unpolarized optical feedback. We have shown that the total power can display LFF which are associated with drops in power of the dominant linearly polarized mode and bursts in the power of the depressed one. However, for most parameter values the VCSEL output does not display LFF, although antiphase dynamics among the two linear polarization components has been found.

In addition, starting from the SFM we have developed a model for a VCSEL subject to optical feedback that allows to include in a simple way all reflections in the external cavity, with a minimal memory cost from the computational point of view. In the deterministic limit the laser with feedback displays a transition from a stable state to a quite irregular one if the current is increased well above the solitary laser threshold. Such a state is presumably connected to the coherence collapse known from edge emitters. When noise is added, LFF-like drops in both the total power and in that of the dominant polarization component are observed closer to (but still above) the solitary laser threshold; these drops are accompanied by bursts of power in the depressed polarization mode, and the observed dynamics for the different current values is qualitatively similar to the experimental observations. We attribute the disagreement among the current values for the observation of LFF to the fact that the model for the interaction among the optical field and the carriers in the active region does not include the spectral dependence of the gain and refractive index into account, and current work is under progress to include it.

ACKNOWLEDGMENTS

T.A. gratefully acknowledges support by the Alexander von Humboldt foundation. S. B. acknowledges financial support from CICYT (Spain) under project TIC98-0418. J. R. T. acknowledges financial support from DGICYT (Spain) under project SAB95-0644.

VI. APPENDIX

The case considered here corresponds to a single-mode VCSEL which, due to growth-induced stresses, presents some small amount of birefringence and dichroism. The main effect of small birefringence is to induce a frequency shift of the two linear polarization orientations of the fundamental mode, leaving the mode profile almost equal to that of the perfect waveguide [27]. Then, each Fourier component of the electric field distribution inside the VCSEL cavity can be written as

$$\mathcal{E}_{\pm}(\omega, z, \rho) = A_{\pm}(\omega)\Psi_{\omega}(z)U_{\omega}(\rho) \; . \tag{12}$$

In this equation, $A_\pm$ is the amplitude of each circular polarization component of the field, $\Psi(\omega, z)$ is the longitudinal field distribution, and $U_\omega(\rho)$ is the modal profile in the perfect waveguide, which extends between the top and bottom Bragg mirrors.

The perfect waveguide is considered to have cylindrical symmetry, and for simplicity we take it longitudinally homogeneous. Then, $U_\omega(\rho)$ is given by

$$\nabla_\perp^2 U_\omega(\rho) + \frac{\omega^2}{c^2}\varepsilon_\omega(\rho)U_\omega(\rho) = \beta_\omega^2 U_\omega(\rho) \ , \tag{13}$$

where c is the speed of light in vacuum, $\varepsilon_\omega(\rho)$ is the distribution of the dielectric function, and β_ω the propagation constant of the mode in the unperturbed waveguide. We assume perfect mode-matching between the field leaving the top mirror and the reinjected field.

The longitudinal field distribution is in turn given by

$$\Psi_\omega(z) = r_1 e^{iqz} + e^{-iqz} \ , \tag{14}$$

where the boundary conditions at the edges of the cavity select the allowed longitudinal wavevectors q,

$$q = M\frac{\pi}{L} + \frac{i}{2L} ln\left(r_1 \frac{r_2 + r_3 e^{i\omega\tau}}{1 + r_2 r_3 e^{i\omega\tau}}\right) \tag{15}$$

$$\equiv q_0 + i\phi(\omega) \ , \tag{16}$$

r_1, r_2 and r_3 being the effective field reflectivities of the bottom, top and external mirror, respectively,and $\tau = 2L_{ext}/c$ the roundtrip time in the external cavity. q_0 corresponds to the wavevector when no external cavity is present,

$$q_0 = M\frac{\pi}{L} + \frac{i}{2L} ln\left(r_1 r_2\right) \ , \tag{17}$$

while $\phi(\omega)$ takes into account the effects of the external cavity,

$$\phi(\omega) = \frac{i}{2L} ln\left(1 + \frac{1 - r_2^2}{r_2}\frac{r_3 e^{i\omega\tau}}{1 + r_2 r_3 e^{i\omega\tau}}\right) \ . \tag{18}$$

We assume that only one of these wavevectors is in the vicinity of the gain peak, hence the VCSEL operates single-longitudinal mode. Substituting (12) into the wave equation for each polarization component of the field, and assuming that they are around the carrier frequency Ω given by $M(\pi/L) = \beta(\Omega)$, the frequency components of the slowly-varying amplitudes in each polarization component are given by

$$-iuA_{\pm}(u) = -\kappa A_{\pm}(u) + i\Gamma P_{\pm}(u) - (\gamma_a + i\gamma_p)A_{\mp}(u) + \frac{c}{n_g}\phi(\Omega + u)A_{\pm}(u) \; , \tag{19}$$

where $\kappa = 1/(2\tau_p)$, τ_p being the photon lifetime in the solitary VCSEL cavity, γ_a and γ_p are the dichroism and birefringence, respectively, and $n_g = (d\beta/d\omega)^{-1}_{\omega=\Omega}$ is the group index at the carrier frequency. $P_{\pm}$ is proportional to the carrier-induced electric dipole density in each of the polarizations, and describes the carrier-induced gain and dispersion. Finally, Γ is the field confinement factor to the active region for the carrier frequency Ω.

In order to obtain a time-evolution equation for the field amplitudes, we must Fourier transform back to the time domain, but the presence of the external cavity (through $\phi(\Omega+u)$) does not allow us to obtain a closed form for the evolution equation. The usual approach is then to consider that the reflectivity of the external mirror is very small, and to expand $\phi(\Omega + u)$ to first order in r_3, which amounts to consider only one reflection in the external mirror and leads to the well known Lang and Kobayashi approximation [21]. Unfortunately, this approximation is not justified for VCSELs because of the high reflectivities of the Bragg mirrors, and it is essential to include multiple reflections [14]. However, the high reflectivity of the Bragg mirror allows us to find an alternative solution to the problem. If the lasing mode is close to the center of the stop band, then $r_2 \approx 1$, so $(1 - r_2^2)/r_2$ is a small quantity regardless of r_3. Hence, for a VCSEL we have that

$$\phi(\Omega + u) = \frac{1}{2L} ln\left(1 + \frac{1 - r_2^2}{r_2}\frac{r_3 e^{i\Omega\tau}e^{iu\tau}}{1 + r_2 r_3 e^{i\omega\tau}}\right) \tag{20}$$

$$\approx \frac{1}{2L}\frac{1 - r_2^2}{r_2}\frac{r_3 e^{i\Omega\tau}e^{iu\tau}}{1 + r_2 r_3 e^{i\Omega\tau}e^{iu\tau}} \; . \tag{21}$$

Substituting it into (19), multiplying both sides by $1 + r_2 r_3 e^{i\Omega\tau}e^{iu\tau}$, and Fourier transforming to the time domain, we find

$$R_{\pm}(t) + r_2\hat{r}_3 R_{\pm}(t - \tau) = \frac{c}{2n_g L}\hat{r}_3\frac{1 - r_2^2}{r_2}A_{\pm}(t - \tau) \; , \tag{22}$$

where $\hat{r}_3 = r_3 e^{i\Omega\tau}$ is the effective amplitude reflectivity of the external mirror into the VCSEL cavity including the optical phase change after one external cavity roundtrip, and

$$R_{\pm}(t) = d_t A_{\pm}(t) + \kappa A_{\pm}(t) - i\Gamma P_{\pm}(t) + (\gamma_a + i\gamma_p) A_{\pm}(t) \ . \tag{23}$$

The description of the system is completed with the evolution of the material variables. We take the same model as in [20], which has been extensively studied and provides a good qualitative framework for the description of the VCSEL properties. The only difference with [20] is that we consider nonlinear gain saturation. Then, the electric-dipole density is given by

$$P_{\pm} = -g(\alpha + i) \frac{N_{\pm} - N_t}{1 + s|A_{\pm}|^2} A_{\pm} \ , \tag{24}$$

which is obtained by assuming that birefringence is small enough for the two polarization components have almost the same modal gain g, α factor, transparency carrier density N_t and nonlinear gain saturation coefficient, s. $N_{\pm}$ is the density of carriers with spin down (spin up) within the active region.

REFERENCES

[1] For a review see K. Petermann, IEEE J. Selected Topics in Quantum Electron. **1**, 480 (1995).

[2] R. W. Tkach and A. R. Chraplyvy, J. Lightwave Technol. **LT-4**, 1655 (1986).

[3] A.P Bogatov, P.G. Eliseev, L.P. Ivanov, A.S. Logginov, M. A. Manko, K.Ya Senatorov, IEEE J. Quantum Electron **9**, 392 (1973).

[4] D. Lenstra, B. H. Verbeek and A. J. den Boef, IEEE J. Quantum Electron. **QE-21**, 674 (1985).

[5] W. W. Chow, K. D. Choquette, M. H. Crawford, K. L. Lear and G. R. Hadley, IEEE J. Quantum Electron. **33** 1810 (1997).

[6] C. J. Chang-Hasnain, in *Semiconductor Lasers: Past, Present and Future*, ch. 5, edited by G. P. Agrawal (AIP Press, Woodbury, NY 1995).

[7] T. E. Sale, *Vertical Cavity Surface Emitting Lasers*, Research Studies Press Ltd., Sommerset (UK, 1995).

[8] Z. G. Pan, S. Jiang, M. Dagenais, R. A. Morgan, K. Kojima, M. T. Asom, R. E. Leibenguth, G. D. Guth and M. W. Focht, Appl. Phys. Lett. **63**, 2999 (1993).

[9] J. Jewell, Laser Focus World (May 1990), p. 151.

[10] U. Fiedler and K. J. Ebeling, IEEE J. Selected Topics in Quantum Electron. **1**, 443 (1995).

[11] Y. C. Chung and Y. H. Lee, IEEE Photon. Technol. Lett. **3**, 597 (1991).

[12] S. Jiang, Z. Pan, M. Dagenais, R. A. Morgan and K. Kojima, IEEE Photon. Technol. Lett. **6**, 34 (1994); S. Jiang, M. Dageanis and R. A. Morgan, IEEE Photon. Technol. Lett. **7**, 738 (1995).

[13] J. Dellunde, A. Valle and K. A. Shore, J. Opt. Soc. Amer. B **13**, 2477 (1997).

[14] J. Y. Law and G. P. Agrawal, IEEE J. Selected Topics in Quantum Electron. **3**, 353 (1997).

[15] F.Robert, P. Besnard, M. L. Chares and G. M. Stephan, IEEE J. Quantum Electron. **33**, 2231 (1997); P. Besnard, F. Robert, M. L. Chares and G. M. Stephan, Phys. Rev. A **56**, 3191 (1997).

[16] H. Li, A. Hohl, A. Gavrielides, H. Hou and K. D. Choquette, Appl. Phys. Lett. **72**, 2355 (1998).

[17] N. A. Loiko, A. V. Naumenko and N. B. Abraham, Quantum and Semiclass. Opt. **10**, 125 (1998).

[18] C. Masoller and N. B. Abraham, preprint.

[19] M. San Miguel, Q. Feng and J. V. Moloney, Phys. Rev. A **54**, 5386 (1986).

[20] J. Martín-Regalado, M. San Miguel, N. B. Abraham and F. Prati, Opt. Lett. **21**, 351 (1996); *ibid.*, IEEE J. Quantum Electron. **33**, 765 (1997); J. Martín-Regalado, J. L. A. Chilla, J. J. Rocca and P. Brusenbach, Appl. Phys. Lett. **70**, 3350 (1997).

[21] R. Lang and K. Kobayashi, IEEE J. Quantum Electron. **QE-16**, 347 (1980).

[22] J. Jewell, J. P. Harbison, A. Scherer, Y. H. Lee and L. T. Florez, IEEE J. Quantum Electron. **27**, 1332 (1991); A. K. J. van Doorn, M. P. van Exter, and J.P Woerdman, Appl. Phys. Lett. **69**, 1041 (1996).

[23] P. S. Spencer, C. R. Mirasso, and K. A. Shore, Photon. Technol. Lett. **10**, 191 (1998).

[24] G. Huyet, S. Balle, M. Giudici, C. Green, G. Giacomelli and J. R. Tredicce, Optics Commun. **149**, 341 (1998).

[25] G. Huyet, S. P. Hegarty, M. Giudici, B. de Bruyn, J. G McInerney, Europhys. Lett. **40**,

619 (1997).

[26] G. Vaschenko, M. Giudici, J. J. Rocca, C. S. Menoni, J. R. Tredicce and S. Balle, Phys. Rev. Lett. **81**, 5536-5539 (1998).

[27] A. Valle, J. Sarma and K. A. Shore, IEEE J. Quantum Electron. **31**, 1423 (1995).

FIGURES

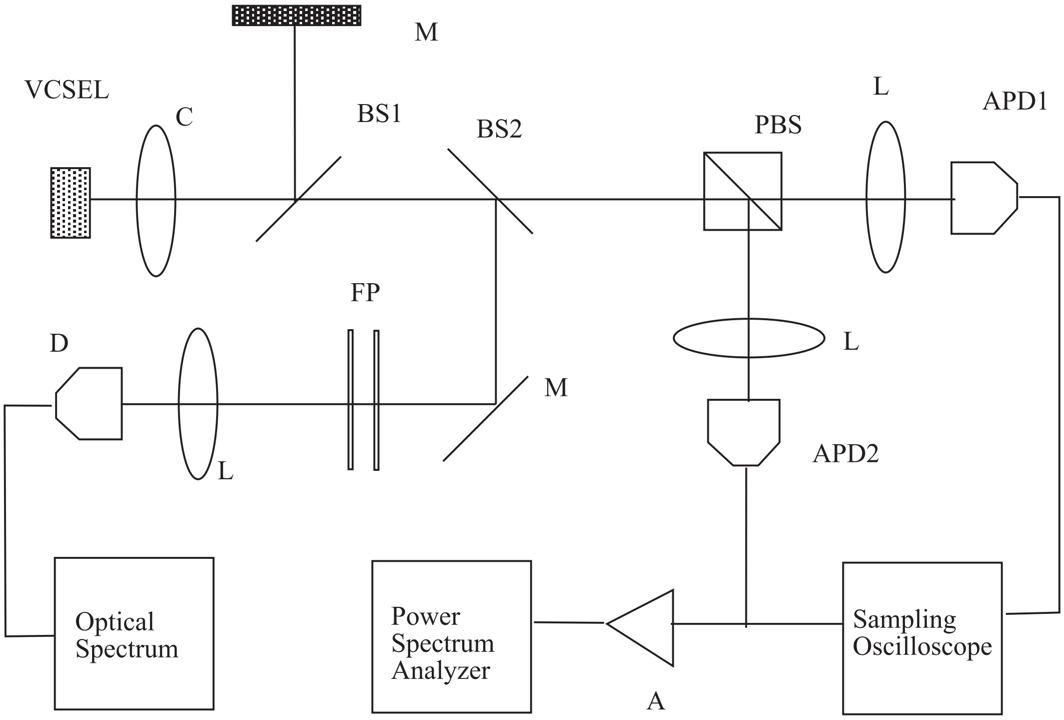

FIG. 1. Schematic experimental setup for high feedback: C collimator, BS beam splitter, PBS polarizing beam splitter, M mirror, L lens, APD avalanche photodiode, D broad area slow detector, FP plano-planar scanning Fabry Perot, A amplifier.

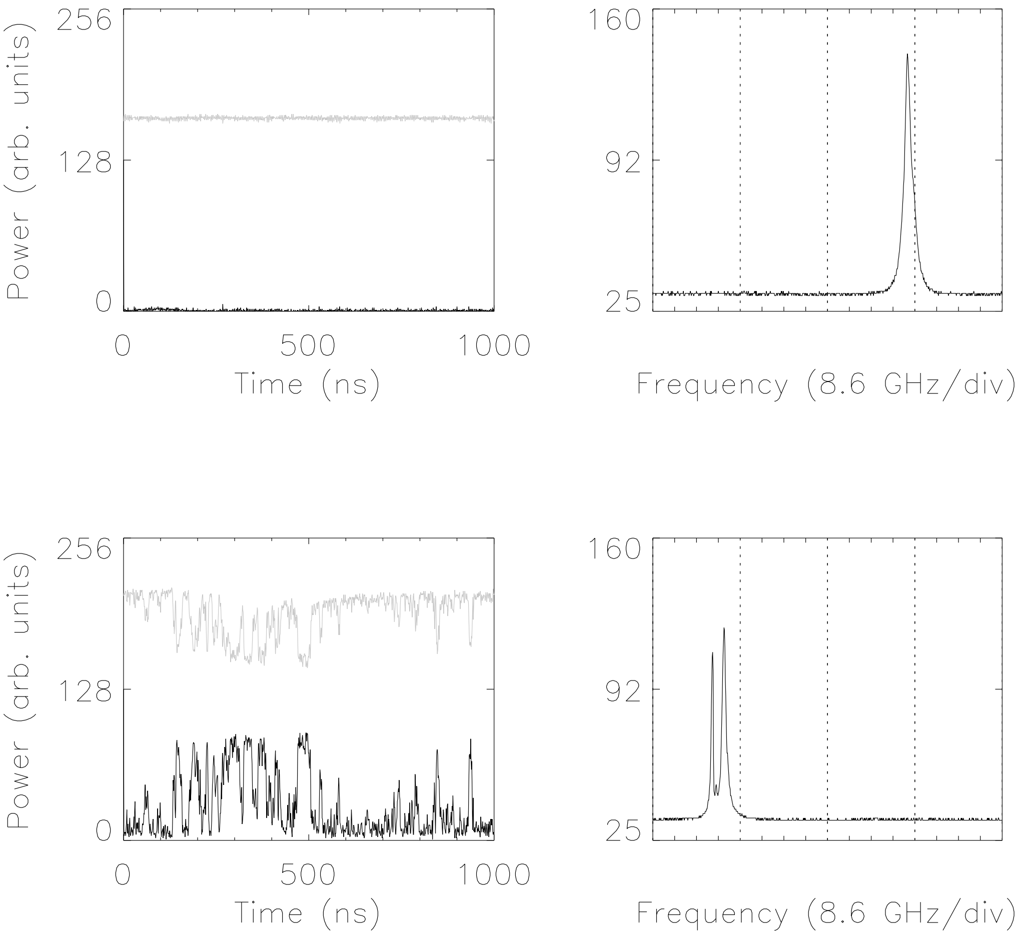

FIG. 2. Polarization resolved dynamics of solitary laser for current 3.01 mA (upper left panel) and 4.11 mA (lower left panel). The right panels display the corresponding optical spectra, with frequency increasing from left to right.

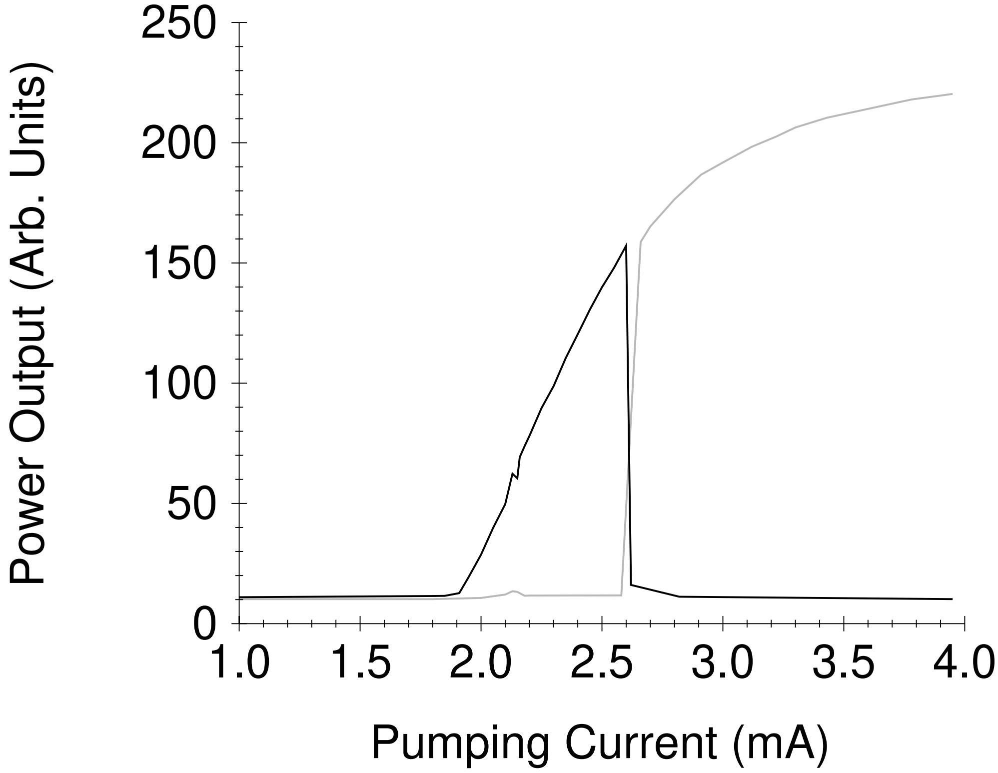

FIG. 3. Polarization resolved LI-curve of the VCSEL in the high-feedback configuration.

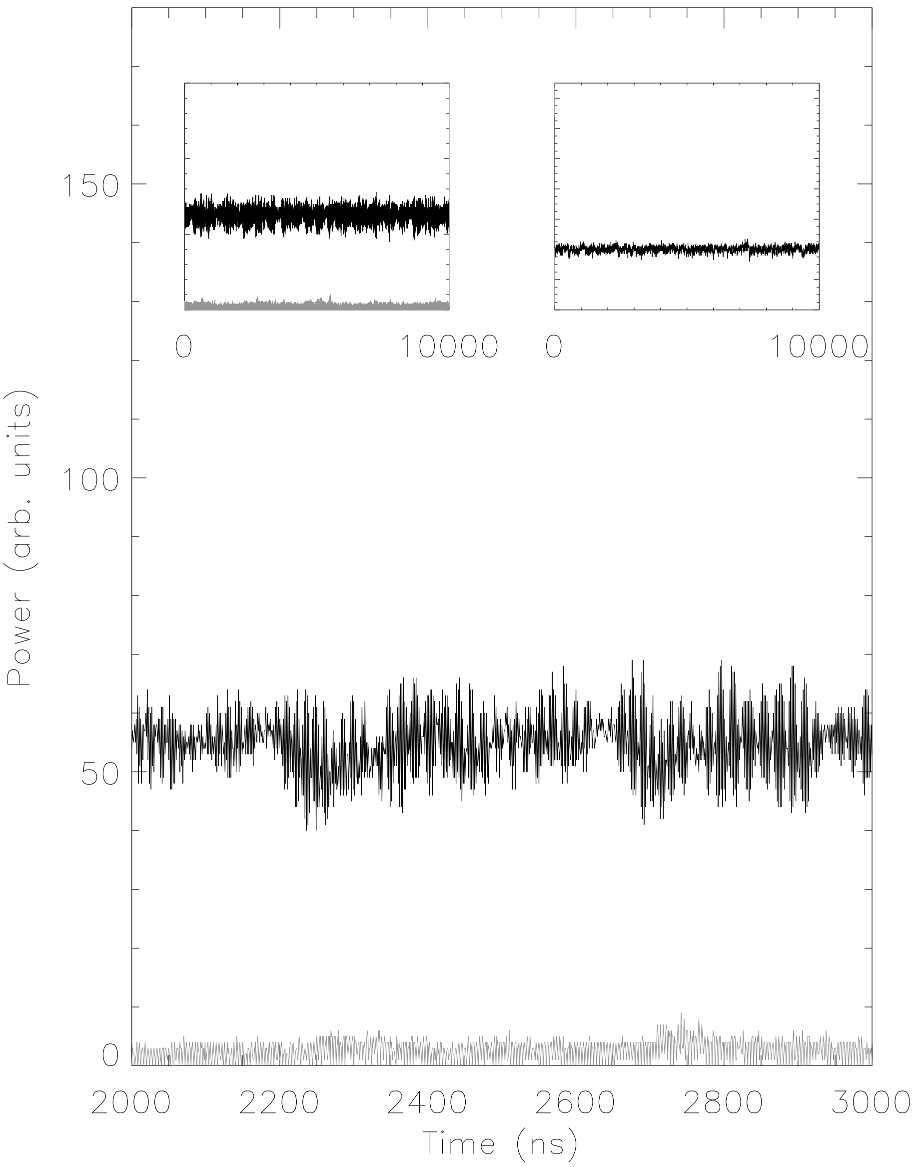

FIG. 4. Polarization-resolved power emitted by the VCSEL in the high-feedback configuration for current injection $I = 2.02$ mA. Left panel: Long time trace of the polarization resolved powers. Right panel: Long time trace of the total power.

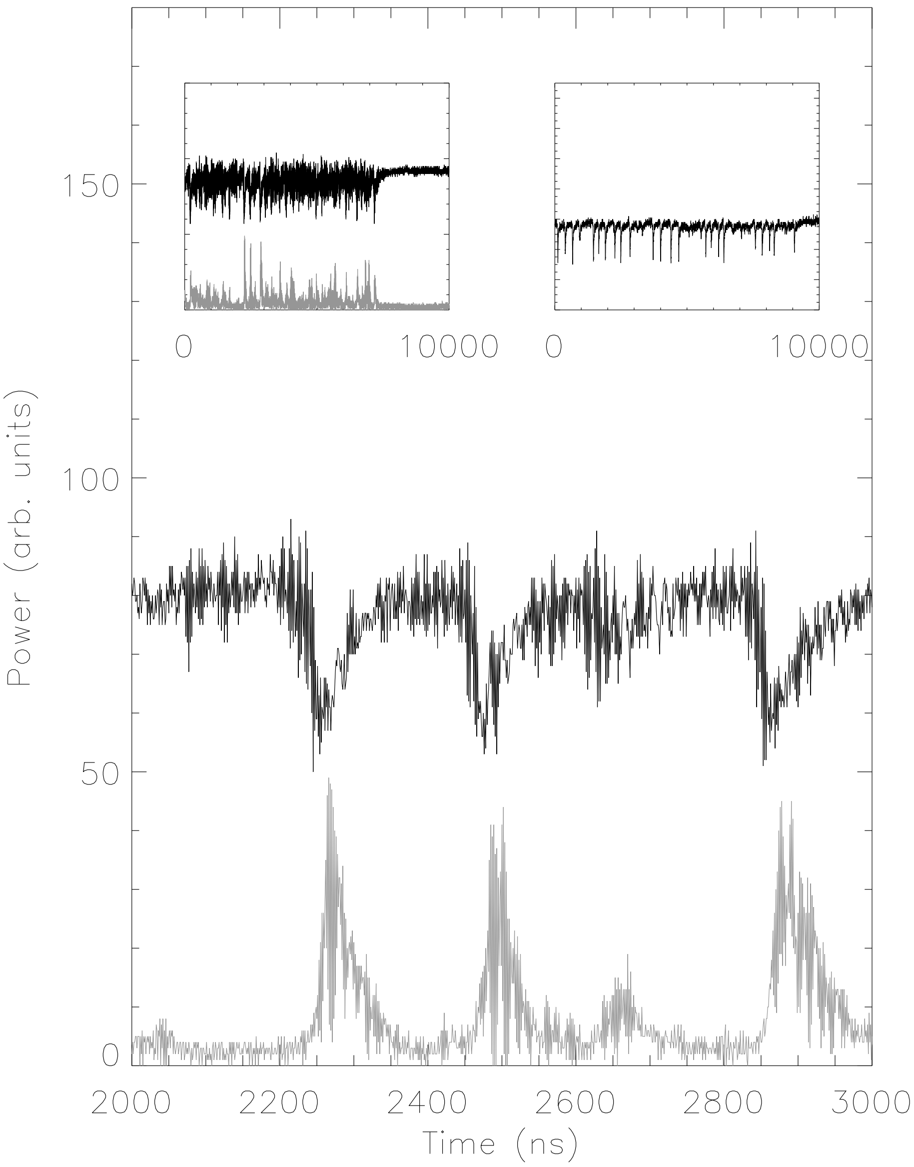

FIG. 5. Same as Fig. 4 but for $I = 2.12$ mA.

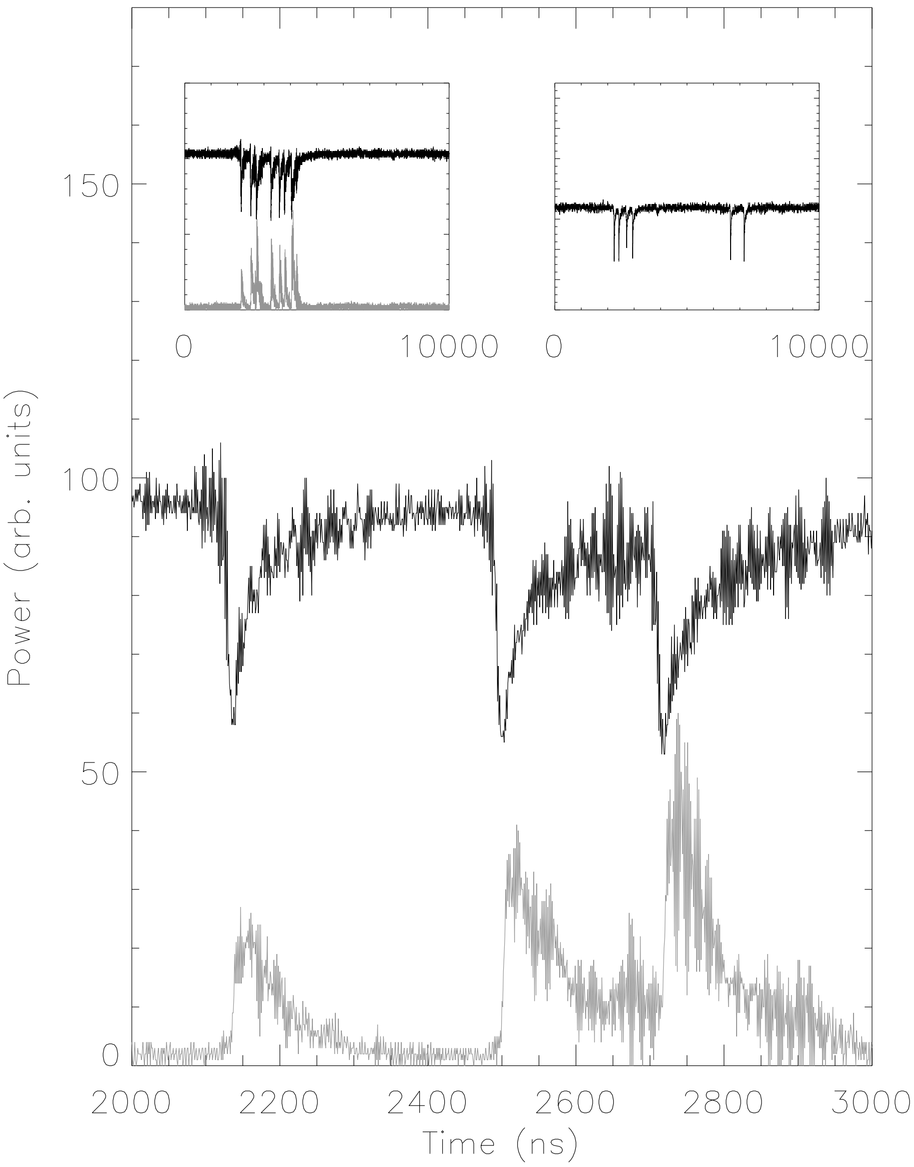

FIG. 6. Same as Fig. 4 but for $I = 2.19$ mA.

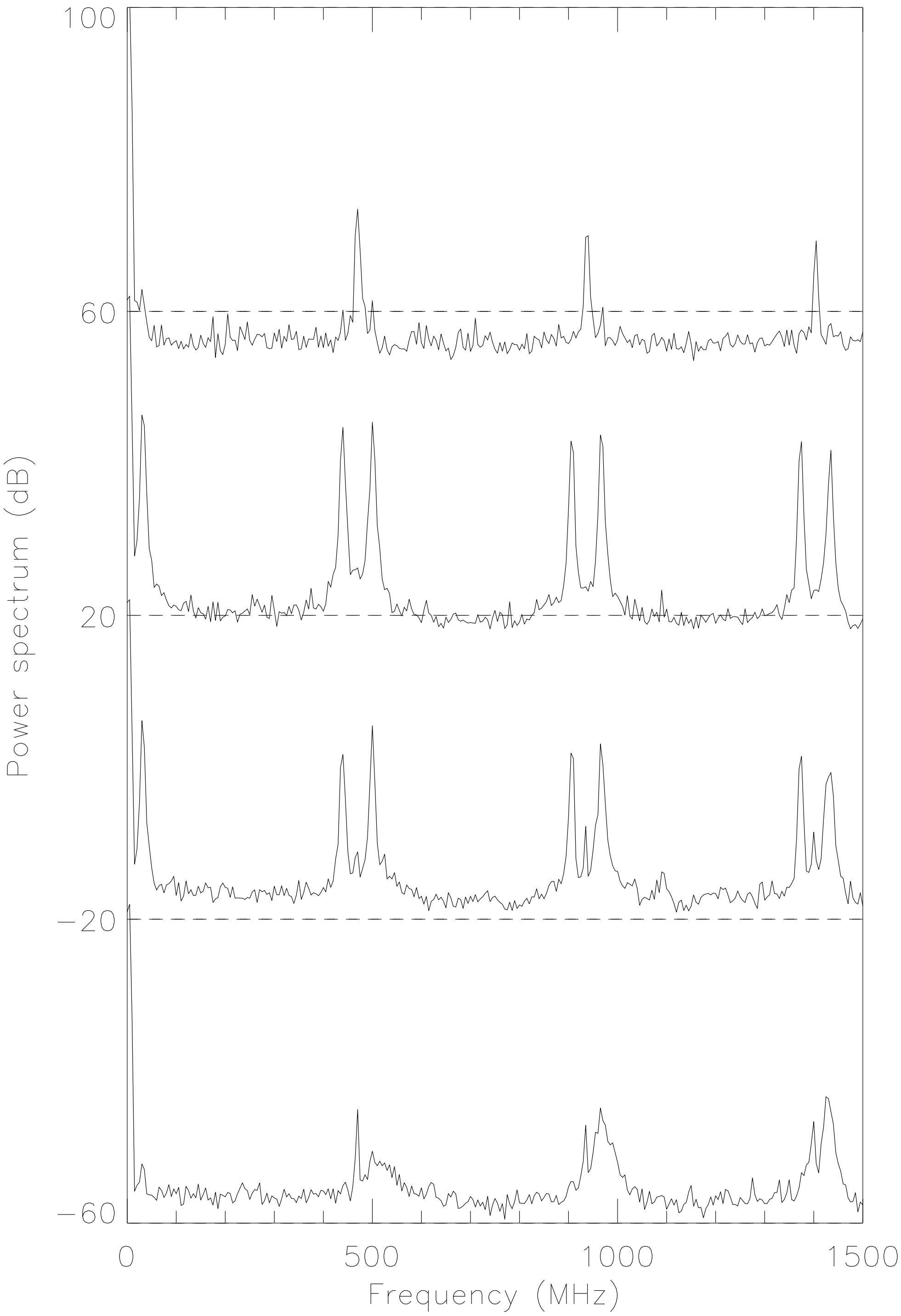

FIG. 7. RF Power spectrum of the VCSEL output when $I = 2.36$ mA for different rotation angles of the $\lambda/2$-waveplate: a) 0^o, b) 26^o, c) 66^o and d) 90^o. The different traces have been offset for clarity, and the broken line denotes the -60 dB level for each trace.

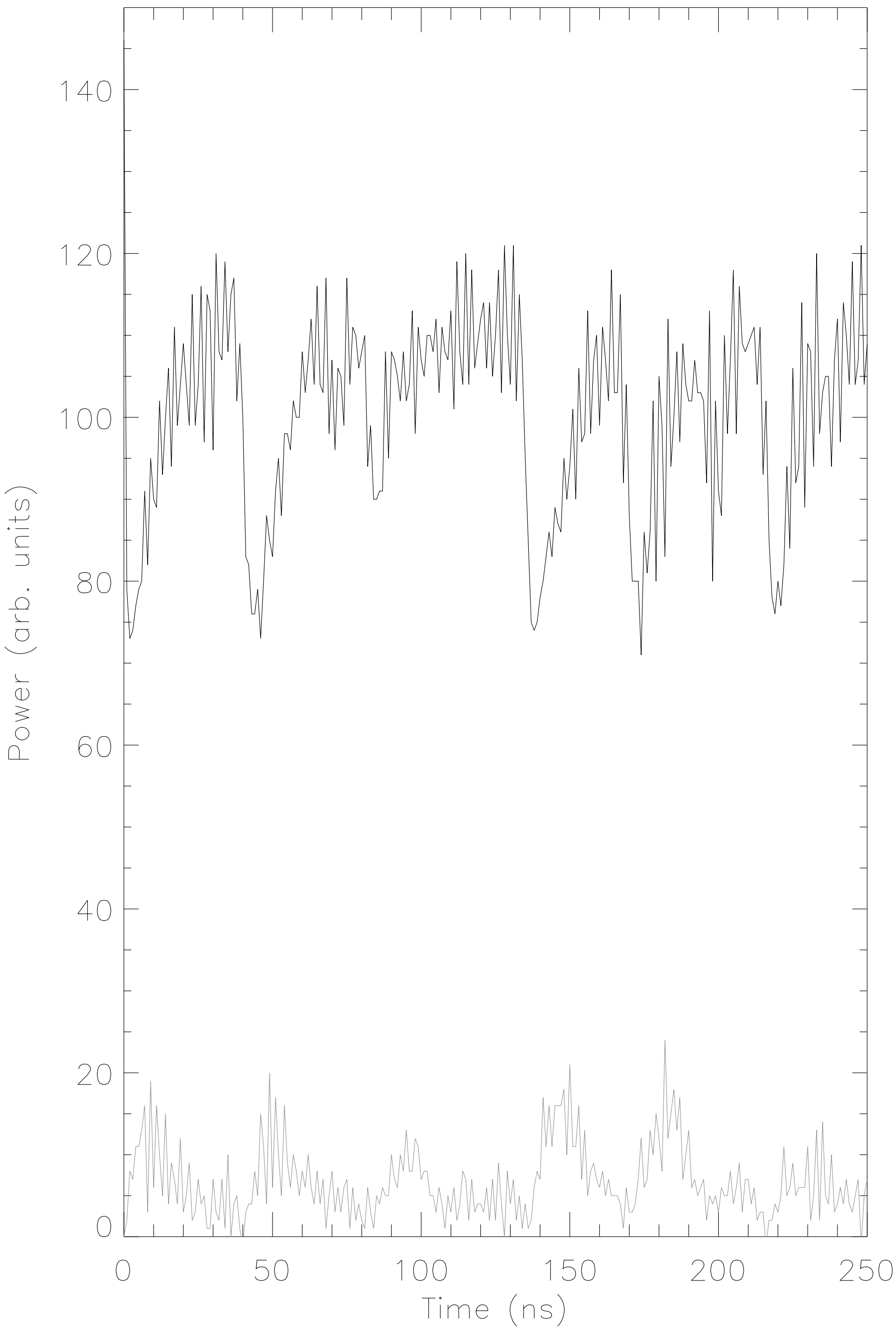

FIG. 8. Polarization resolved time series for the low-feedback configuration when $I = 3.09$ mA.

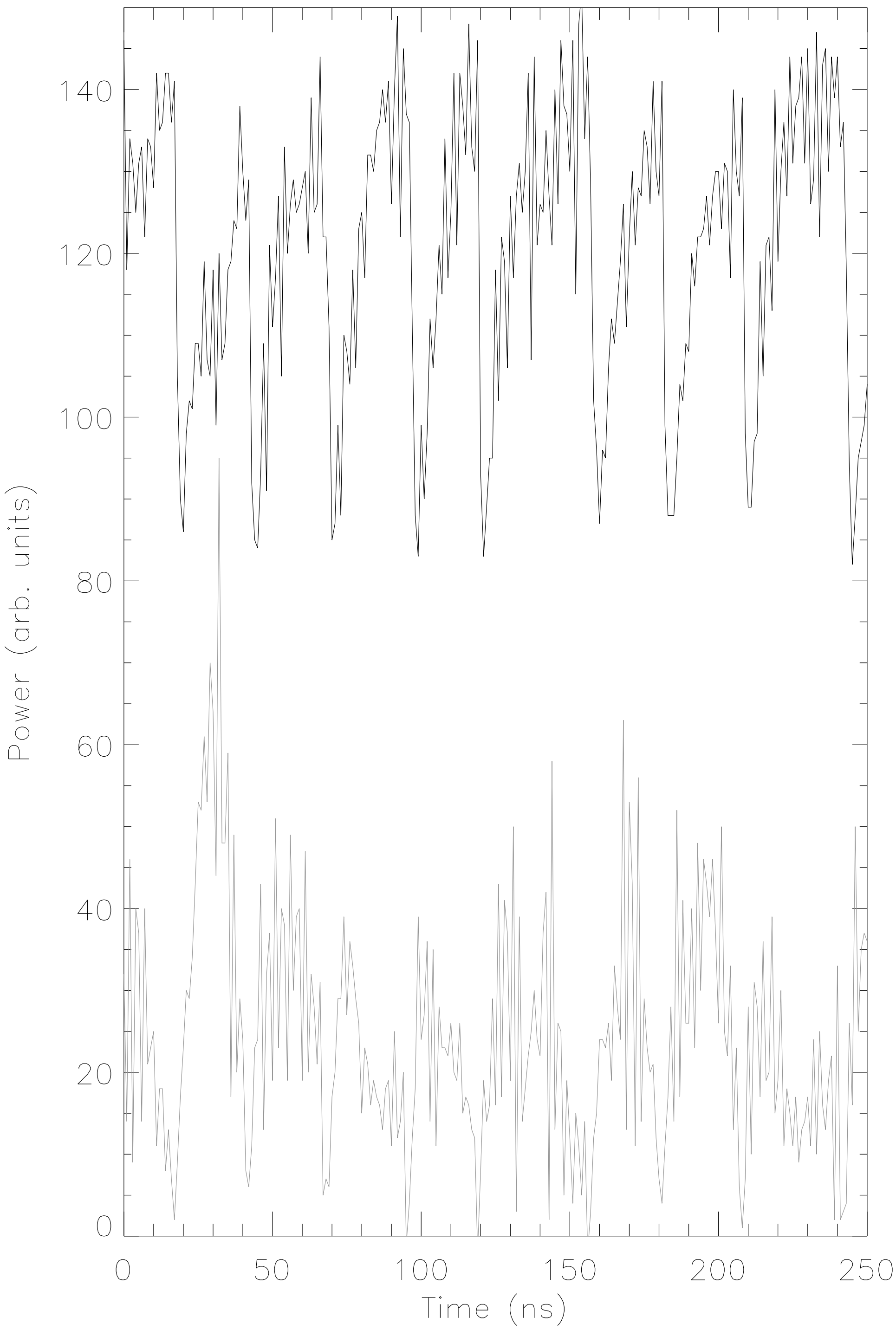

FIG. 9. Polarization resolved time series for the low-feedback configuration when $I = 3.16$ mA.

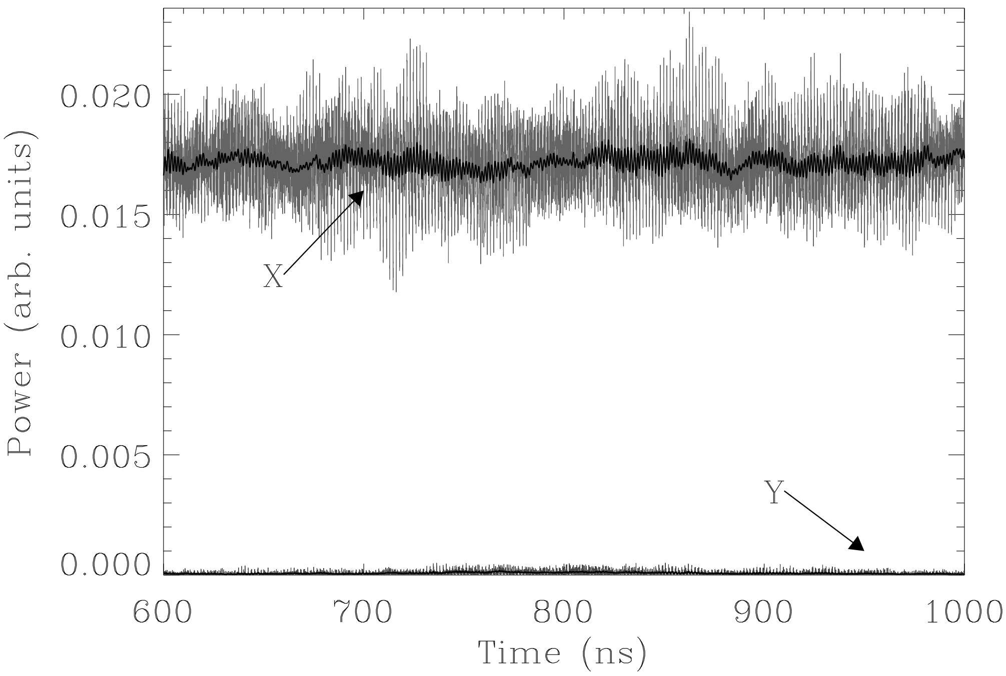

FIG. 10. Polarization resolved time traces as obtained by numerical integration of the theoretical model for $\mu = 0.905$ and a threshold reduction $\sim 12\%$. The grey trace corresponds to the unfiltered output, while the black trace is obtained after low-pass filtering with a second order Butterworth filter of 500 MHz bandwidth.

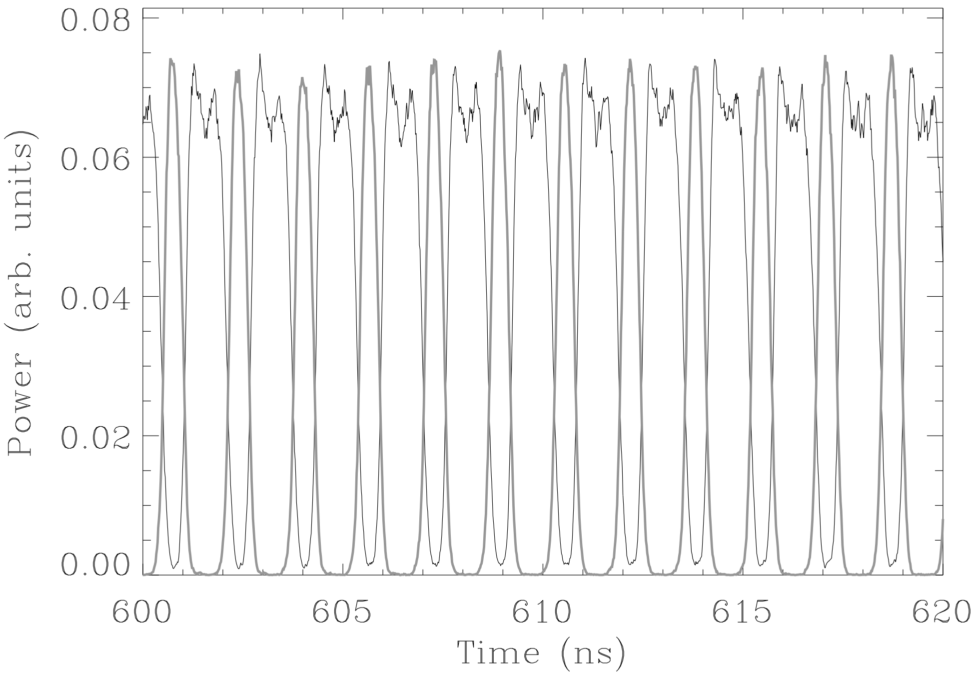

FIG. 11. Unfiltered traces of the power in the X- (black) and Y-polarization (grey) orientations when the current is raised until $\mu = 0.95$.

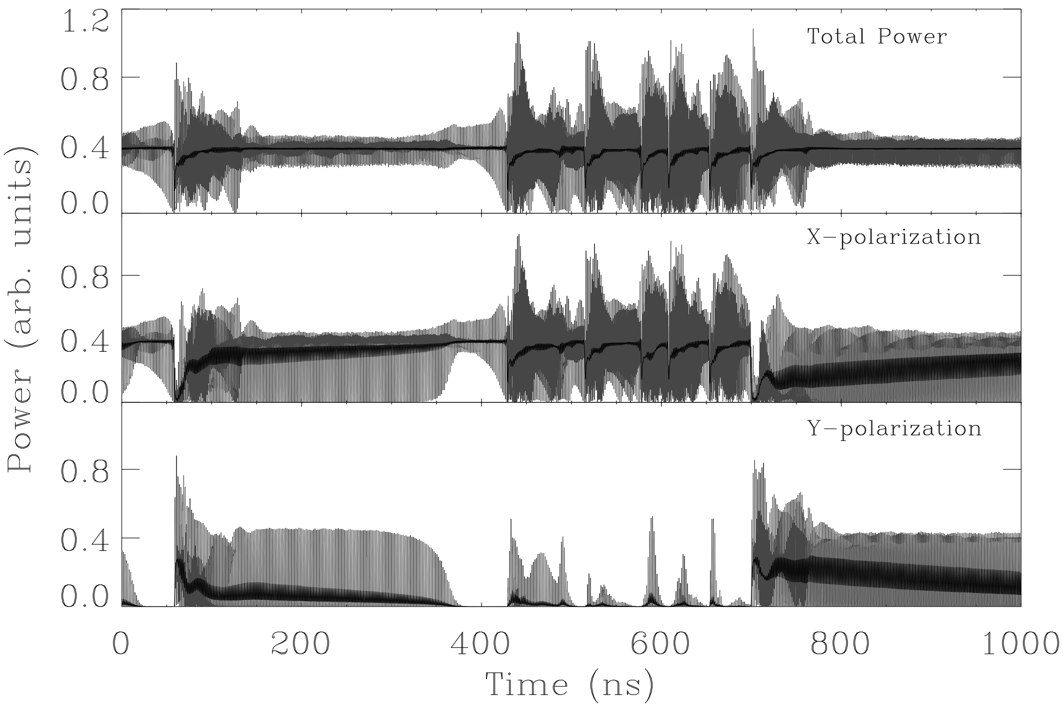

FIG. 12. Same as Fig. 10, but for $\mu = 1.25$.

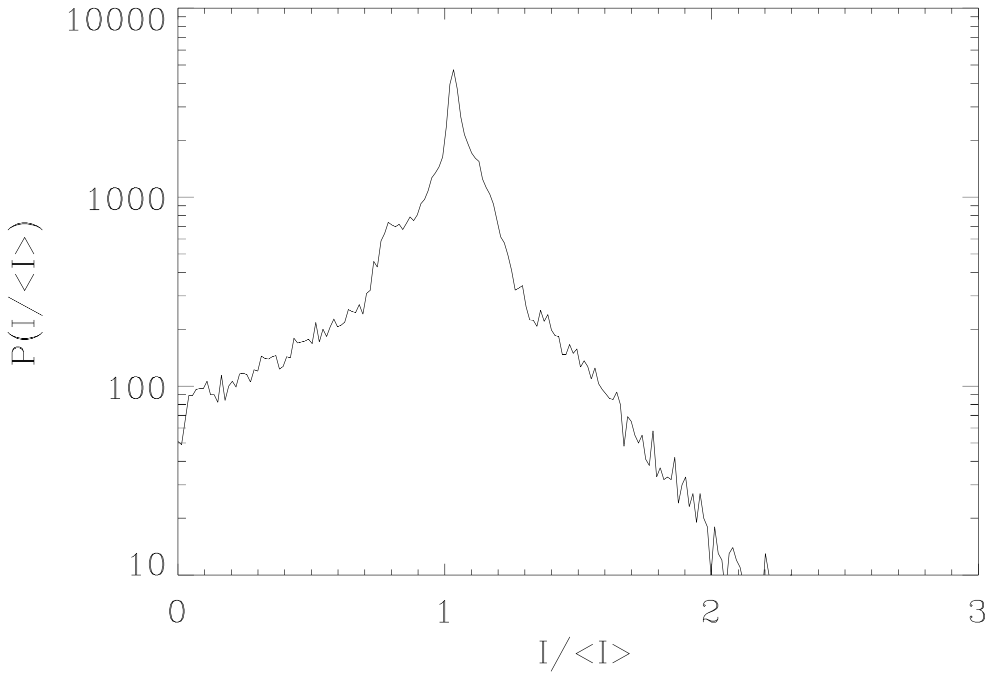

FIG. 13. Histogram of the values of the total power for $\mu = 1.25$ during the time span corresponding to Fig. 12.

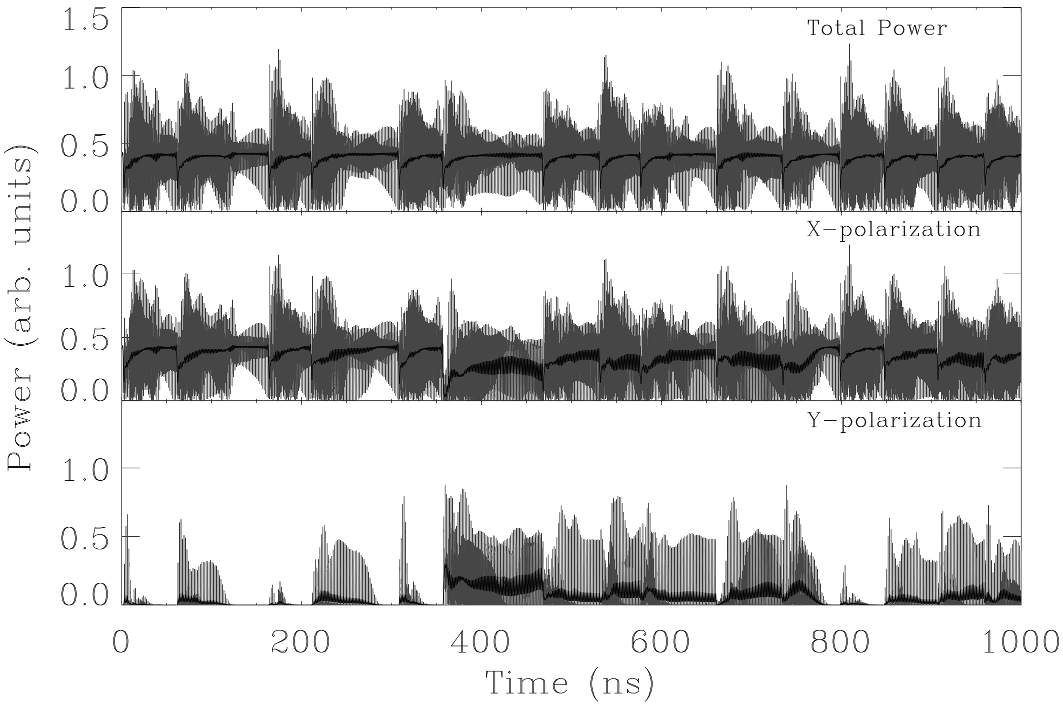

FIG. 14. Same as Fig. 10, but for $\mu = 1.5$.

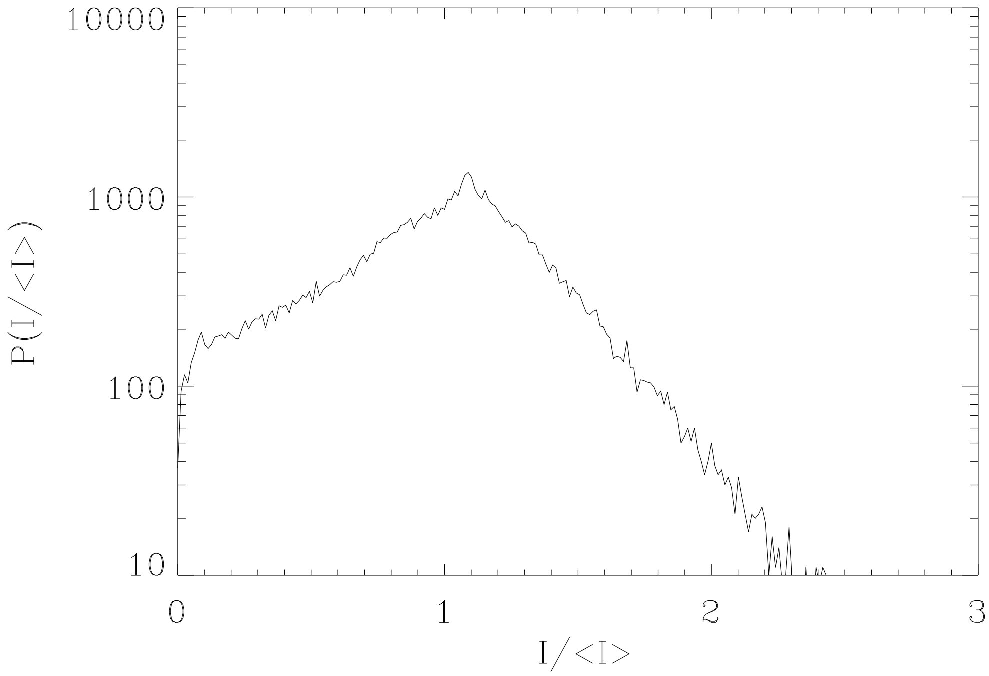

FIG. 15. Histogram of the values of the total power for $\mu = 1.5$ during the time span corresponding to Fig. 14.